



PERGAMON

Micron 32 (2001) 757–764

micron

www.elsevier.com/locate/micron

Contributions of atom probe tomography to the understanding of nickel-based superalloys[☆]

M.K. Miller^{*}

Microscopy and Microanalytical Sciences Group, Metals and Ceramics Division, Oak Ridge National Laboratory, P.O. Box 2008, Oak Ridge, TN 37831-6136, USA

Abstract

Atom probe tomography enables atomic level microstructural characterization to be performed on complex engineering materials such as superalloys. The technique provides information on the size, morphology and compositions of coexisting phases, the solute partitioning of the elements between the phases, and solute segregation to interfaces and grain boundaries. This information leads to a more complete understanding of nickel-based superalloys. The types of atomic level information that may be obtained with atom probe tomography are illustrated with examples of the formation of fine γ' precipitates within the central region of the γ' phase in PW 1480, the evolution of the dual γ'/γ'' nature of secondary precipitates in alloy 718, the interphase precipitation of the γ' phase at the primary $\gamma''-\gamma$ interface in alloy 718, and the quantification of the level and spatial extent of the boron segregation at grain boundaries in a nickel–molybdenum superalloy. Published by Elsevier Science Ltd.

Keywords: Superalloys; Atom probe tomography; Precipitation; Grain boundary segregation

1. Introduction

Nickel-based superalloys are a technologically important class of commercial engineering alloys that are used in elevated temperature environments such as gas turbines for the aerospace industry and land-based applications. Many different types of superalloys have been designed for a variety of applications. In order to obtain a desired set of properties, many different elements are normally added to superalloys. For example, aluminum promotes the formation of γ' precipitates and ensures a dense continuous layer of alumina on the surface, chromium provides excellent corrosion resistance, tantalum confers good creep strength, good oxidation resistance and reduces casting defects, tungsten improves the strength of the γ matrix, and cobalt has good stacking fault energy.

Superalloys derive their good mechanical properties at elevated temperatures from a high volume fraction (up to 70%) of fine ordered precipitates in a face centered cubic γ matrix. Many superalloys are designed to promote the

formation of $L1_2$ -ordered γ' (Ni_3Al) precipitates. However, some widely used superalloys, such as alloy 718, use niobium additions and lower aluminum levels to promote the formation of DO_{22} -ordered γ'' ($\text{Ni}_3(\text{Nb},\text{Ti},\text{Al})$) precipitates. Another superalloy, HAYNES[®] 242[™] alloy, is strengthened with ordered nickel–molybdenum precipitates.

The techniques of atom probe tomography (APT) and atom probe field ion microscopy (APFIM) have been applied to many different commercial nickel-based superalloys in order to characterize the microstructure at the atomic level. Most of these studies have been reviewed previously (Miller et al., 1996; Blavette et al., 2000). The main types of microstructural characterization that have been performed with these powerful microanalytical techniques on these alloys are the determination of the size, morphology and compositions of the coexisting phases as a function of the multistage heat treatments, the investigation of the solute concentration profiles at interfaces, and the quantification of the solute segregation at grain boundaries. Information such as the partitioning of the solute elements between the coexisting phases and segregation to interfaces is important so that the composition and processing of the alloy can be optimized both in terms of the properties and also production costs. In addition to these types of characterizations, the microstructural development of single-crystal nickel-based superalloys during welding has

[☆] The submitted manuscript has been authored by a contractor of the US Government under contract No. DE-AC05-96OR22464. Accordingly, the US Government retains a nonexclusive, royalty-free license to publish or reproduce the published form of this contribution, or allow others to do so, for US Government purposes.

^{*} Tel.: +1-865-574-4179; fax: +1-865-241-3650.

E-mail address: millermk@ornl.gov (M.K. Miller).

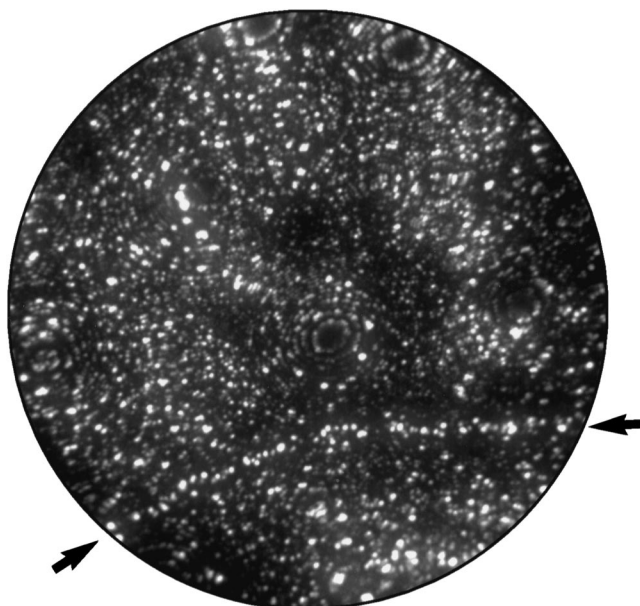


Fig. 1. Field ion micrograph of a decorated grain boundary in a nickel–molybdenum superalloy.

also been studied in PWA 1480 (Babu et al., 1996a) and CMSX-4 (Babu et al., 1996b) superalloys. This type of information should also permit improved superalloys to be designed.

The types of characterizations that may be performed with atom probe tomography are illustrated in this paper with a series of examples including the formation of fine γ precipitates within the central region of the γ' phase in PW 1480, the evolution of the dual γ'/γ'' nature of secondary precipitates in alloy 718, the interphase precipitation of the γ' phase at the primary $\gamma''-\gamma$ interface in alloy 718, and the quantification of the level and spatial extent of the boron segregation at grain boundaries in a nickel–molybdenum superalloy.

2. Atom probe tomography

The technique of atom probe tomography (Miller, 1986) is able to determine the spatial coordinates and the identities of the individual atoms in a metal specimen with close to atomic resolution (~ 0.3 nm). The surface atoms of a cryogenically-cooled needle-shaped specimen are individually ionized by the application of a short duration (10 ns) high voltage pulse superimposed on a standing voltage on the specimen. These ions are then radially projected from the specimen in a time-of-flight mass spectrometer and detected with a single atom position-sensitive detector. In these three-dimensional atom probe (3DAP) instruments, the typical magnification of the specimen surface at the single atom detector is ~ 5 million times. The identities of the ions are determined from their flight times in a time-of-flight mass spectrometer due to the equivalence of the potential energy

of the ion on the surface prior to field ionization and its kinetic energy after field evaporation. A full description of the technique may be found in a monograph by Miller (2000).

The 3DAP data used in this paper were obtained in an energy-compensated optical position-sensitive atom probe. Some additional data were obtained in the Oak Ridge National Laboratory's energy-compensated atom probe field ion microscope. In all the examples shown in this paper, the experimental conditions were a specimen temperature of between 50 and 60 K, a pulse fraction of 20% and a pulse repetition rate of 1500 Hz. All field ion micrographs were recorded with neon as the image gas and with a specimen temperature of between 50 and 60 K.

3. Grain boundary segregation

In polycrystalline superalloys, one of the primary concerns is the strength of the grain boundaries. Solute segregation to and phase formation at the grain boundaries during the initial heat treatments and during service may significantly alter these properties. Since the grain size of superalloys is typically extremely large on the basis of atomic dimensions, encountering a grain boundary during random analysis is highly unlikely. Therefore, few atom probe tomography characterizations of grain boundaries have been performed on superalloys (Letellier et al., 1994a,b; Blavette et al., 1996a,b).

An atom probe tomography characterization has been performed on a grain boundary in a nickel–molybdenum alloy. The main alloying components of the HAYNES 242 nickel-based superalloy used in this grain boundary investigation were 16.4 at.% Mo, 9.3% Cr, 1.3% Fe, 0.018% B and $<0.01\%$ P. This superalloy was examined after a heat treatment designed to produce small Ni_2Mo precipitates in a face centered cubic γ matrix.

A field ion image of a region of a grain boundary in this nickel–molybdenum superalloy is shown in Fig. 1. Solute enrichment at the boundary is evident from the large number of brightly-imaging atoms observed in this micrograph. The field ion images also indicated that there was some significant width to the solute enrichment at the grain boundary. A three-dimensional atom map reconstruction of three-dimensional atom probe data that includes a portion of this boundary and a precipitate is shown in Fig. 2. This atom-by-atom reconstruction indicates the positions of the individual molybdenum, boron and phosphorus atoms. The other atom species have been omitted for clarity. The atom map clearly indicates molybdenum enrichment in the precipitate and boron and phosphorus segregation to the grain boundary. Superimposed on this atom map is the $\sim 17\%$ molybdenum isoconcentration surface which indicates the position of the interface between the γ matrix and the Ni_2Mo precipitate and the location of the grain boundary. Composition profiles through these data that were oriented perpendicular

Mo B P

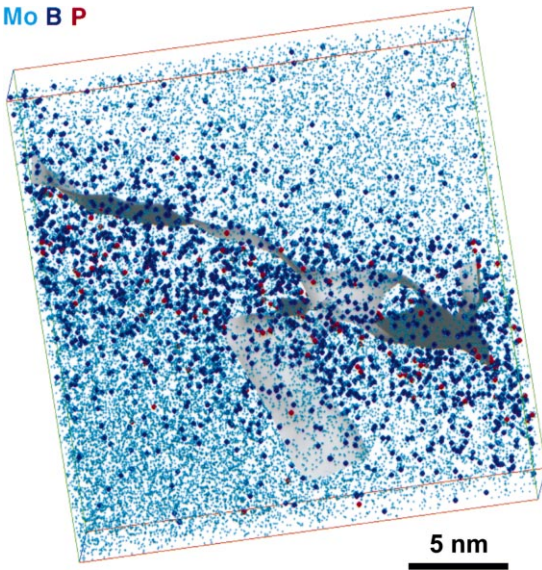


Fig. 2. Atom map of a section of three-dimensional atom probe data that contains a grain boundary in a nickel–molybdenum superalloy. The isoconcentration surface is at 17% Mo and indicates the positions of the grain boundary and a Ni_2Mo precipitate. Boron (blue spheres) and phosphorus (red spheres) enrichments at the grain boundary are clearly evident.

to the grain boundary at a γ – γ section and at a γ –precipitate section are shown in Fig. 3a and b, respectively. Marked enrichments of boron, phosphorus and molybdenum are evident at the grain boundary. The full width at half maximum of the boron enrichment at the grain boundary was approximately 4 nm and the elevated boron level extended for ~ 10 nm into the phases adjacent to the boundary. The simultaneous enrichments of molybdenum and boron may be indicative of the formation of an ultrathin film of molybdenum boride at the grain boundary. In addition, chromium enrichment is observed at the Ni_2Mo precipitate–matrix interface and the Ni_2Mo precipitates contain significant levels of chromium.

4. Precipitation in single crystal PW1480

Single crystal turbine blades were introduced in the early 1980s and have resulted in significant increases in the allowable metal temperatures and rotor speeds. For example, PWA 1480 is designed to operate in an environment where the gas temperature is $\geq 1400^\circ\text{C}$ and the temperature of the metal surface is $>1050^\circ\text{C}$. As these alloys do not require additional elements such as boron, carbon, hafnium and zirconium to strengthen the grain boundaries, their compositions may be refined to produce high incipient melting temperatures and high γ' solvus temperatures. At these elevated temperatures, the properties of the γ' precipitates become increasingly important.

The nominal composition of the PWA 1480 superalloy used in this investigation was Ni–11.7 at.% Cr, 11.3% Al, 5.2% Co, 4.0% Ta, 1.9% Ti and 1.3% W. The material was characterized after a three-step heat treatment of 4 h at 1288°C (1561 K), 4 h at 1079°C (1352 K) and 32 h at 871°C (1144 K). The material was air-cooled to room temperature between each stage of the heat treatment. The first step was a homogenizing and solutioning treatment and the second step was a standard industrial treatment for stabilizing the surface coating used on these turbine blades.

The general microstructure of this single crystal material was coarse ($\sim 0.5 \mu\text{m}$) cuboidal L1_2 -ordered γ' precipitates uniformly distributed in a γ matrix (Miller et al., 1994). Atom probe analysis revealed that chromium, cobalt and tungsten partitioned preferentially to the γ matrix and that aluminum, titanium and tantalum partitioned to the γ' precipitates, as shown in Table 1. Some 10–20 nm diameter secondary γ' precipitates were also observed in the γ matrix after the second stage of the heat treatment (4 h at 1352 K (1079°C)).

A high number density of small (5–10 nm diameter) spherical precipitates were observed in the central regions of the γ' precipitates in material that was given the third step of the heat treatment. The outer 100 nm of the γ' precipitates was denuded with these spherical precipitates. These

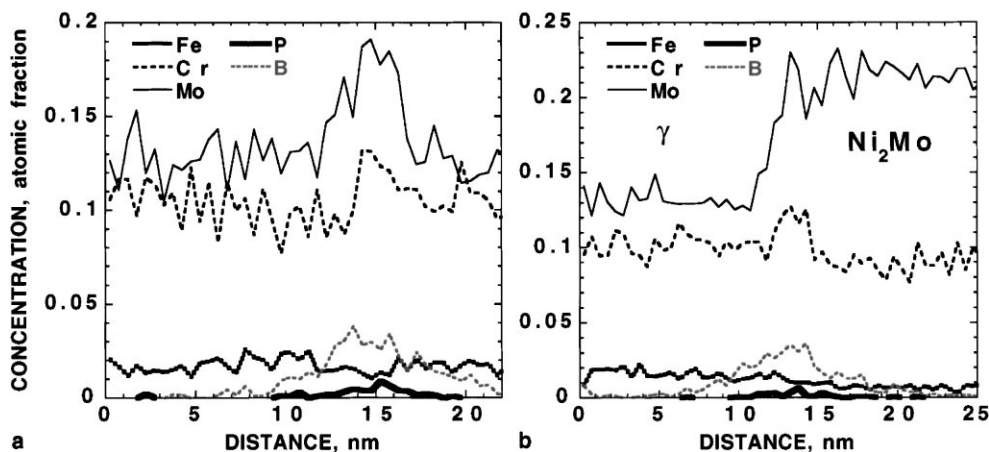


Fig. 3. Composition profiles across the grain boundary shown in Fig. 2: (a) across the γ – γ boundary; (b) across the grain boundary at a γ – Ni_2Mo precipitate section. Boron and phosphorus enrichments at the boundary and precipitate matrix interface are evident.

Table 1

Average compositions of the phase in PWA 1480 after the three stage heat treatment. The balance of each analysis is nickel and the data are in atomic percent

Phase	Cr	Co	Al	Ti	Ta	W
γ matrix	26.2 ± 2.4	11.4 ± 0.4	3.0 ± 0.1	0.3 ± 0.2	1.2 ± 0.8	3.4 ± 0.6
γ' precipitate (interior region)	1.94 ± 0.02	2.92 ± 0.02	14.6 ± 0.05	2.63 ± 0.02	6.45 ± 0.04	0.73 ± 0.01
γ precipitate	36.3 ± 0.28	11.1 ± 0.18	1.7 ± 0.07	0.25 ± 0.03	0.58 ± 0.048	0.74 ± 0.05

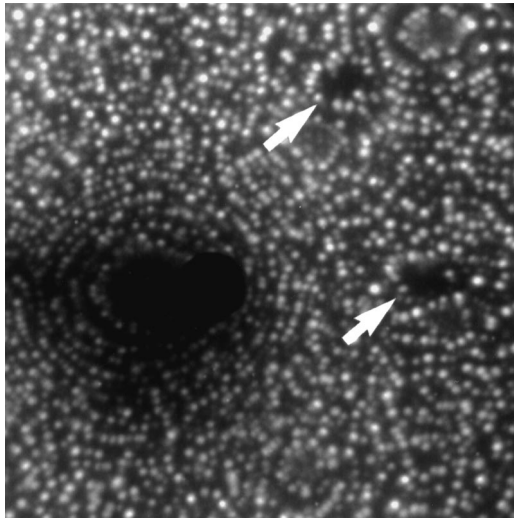


Fig. 4. Field ion micrograph of the central region of a cuboidal γ' precipitate in PWA 1480. Two small darkly-imaging spherical precipitates are evident.

spherical precipitates appear as the small dark regions in the field ion micrograph shown in Fig. 4 and also appear as dark regions in dark field transmission electron micrographs taken with an L_{12} -ordered superlattice reflection (Miller et al., 1994). In addition, no extra spots were observed in the electron diffraction patterns and continuity of planes from the γ phase to the γ' precipitate has been observed in atom maps. Therefore, it is probable that these precipitates have a face centered cubic crystal structure. Atom maps of a central region of a γ' precipitate are shown in Fig. 5. The average compositions of these precipitates are given in Table 1. Enrichments of chromium and cobalt and depletions of aluminum, titanium and tantalum are observed with respect to the surrounding γ' precipitate in the spherical precipitates. The partitioning behavior of the alloying elements is similar to that observed in the γ matrix. However, the chromium level is significantly higher and the aluminum, tantalum and tungsten levels are slightly lower. These differences are probably due to the different environment from which the precipitation occurs and the wide solubility range of the

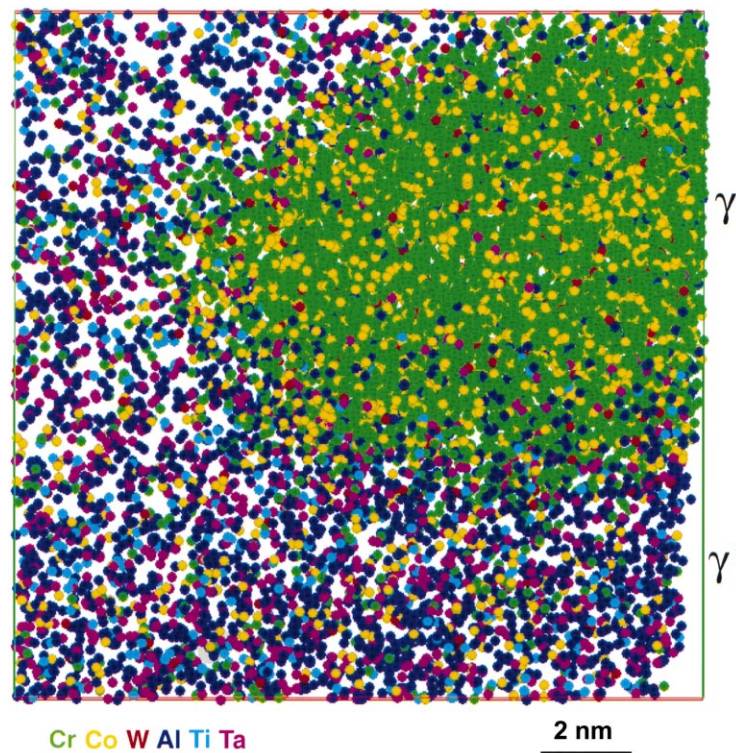


Fig. 5. Atom maps of the central region of a cuboidal γ' precipitate in PWA 1480. Small spherical precipitates are evident. The precipitates are enriched in chromium and cobalt and depleted in aluminum, titanium and tantalum.

γ phase. Therefore, their composition and crystal structure suggest that these precipitates are γ phase. The presence of these γ precipitates within the γ' precipitate provides additional interfacial γ – γ' area which could impede the motion of dislocations and thereby enhance the mechanical properties. Similar features have also been observed in superalloy N18 (Blavette et al., 2000).

5. Precipitation in alloy 718

Alloy 718 is a widely used niobium-containing nickel base superalloy that obtains its high temperature strength from a dispersion of lenticular DO₂₂-ordered γ'' precipitates and roughly spherical secondary precipitates in a γ matrix (Loria, 1989; Burke and Miller, 1989, 1991a; Miller, 1999). The DO₂₂-ordered structure can be described as an L1₂-ordered structure with an $[\frac{1}{2} \frac{1}{2} 0]$ displacement every other 001 plane. In addition, the compositions of the DO₂₂-ordered and L1₂-ordered structures can both be described as Ni₃(Al,Ti,Nb) with different levels of aluminum, titanium and niobium. Atom probe tomography characterization of alloy 718 has been undertaken in order to establish the nature of the secondary precipitates.

The composition of the alloy 718 used in this investigation was Ni–21.8 at.% Cr, 20.3% Fe, 3.2% Nb, 1.81% Mo, 1.15% Ti, 0.96% Al, 0.26% Co and 0.26% C. This material was given a standard heat treatment (A) of 1 h at 1038°C (1311 K). The specimens were water quenched to room temperature between each stage. Transmission electron microscopy, atom probe analysis (Burke and Miller, 1991a; Miller and Burke, 1991) and thermodynamic predictions (Miller, 1999) indicate that the intragranular microstructure is single γ phase at 1038°C (1311 K). Some of this material was subsequently heat treated (AC) for 8 h at 870°C (1143 K). During this stage of the heat treatment, transmission electron microscopy and atom probe field ion microscopy determined that the lenticular primary γ'' precipitates are formed (Burke and Miller, 1991a) in agreement with thermodynamic predictions. A field ion micrograph of a portion of a lenticular γ'' precipitate in the γ matrix is shown in Fig. 6a. Analysis of the compositions of the phases revealed that iron, chromium, molybdenum, and cobalt preferentially partitioned to the γ matrix and niobium, and

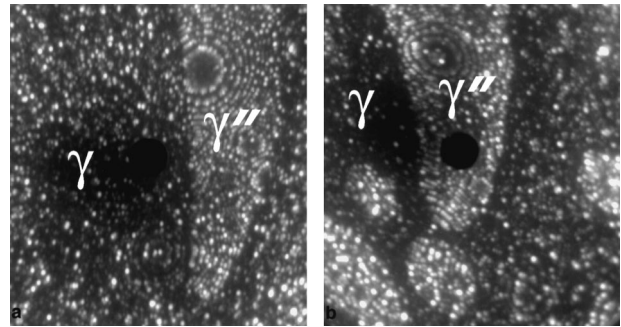


Fig. 6. Field ion micrographs of the microstructure of alloy 718: (a) a primary γ'' precipitate in the γ matrix after the AC heat treatment; (b) a primary γ'' precipitate and three secondary precipitates in the γ matrix after the AC + 8 h at 760°C heat treatment.

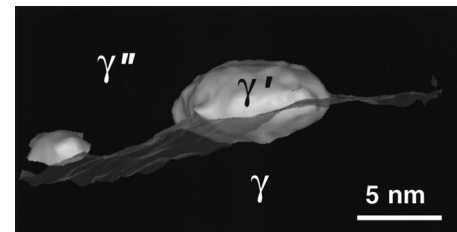


Fig. 7. Isoconcentration surfaces of small γ' precipitates on the surface of a primary γ'' precipitate in alloy 718.

titanium partitioned to the γ'' phase, as shown in Table 2. These observations are in agreement with thermodynamic predictions. Concentration profiles across the interface also revealed enrichments and depletions close to the γ'' precipitate– γ matrix interface. Chromium and titanium exhibited slight depletions and iron a significant enrichment in the γ'' precipitate near the γ matrix. Manganese and aluminum exhibited local enrichment and niobium exhibited a depletion in the γ matrix adjacent to the γ'' precipitate. Carbon exhibited a small local enrichment at the interface. The widths of these local solute enriched and depleted regions ranged from ~ 1 nm for the aluminum and carbon to ~ 5 nm for the other elements.

Some additional phases including a C14 Laves phase, orthorhombic δ (Ni₃Nb) precipitates and coarse MC carbides are also present (Burke and Miller, 1991b). Secondary precipitates are formed in the γ matrix in material that is heat treated at $\sim 760^\circ\text{C}$ (1033 K) or lower temperatures, as

Table 2

Average compositions of the phases in alloy 718 as measured from selected volume analysis of three-dimensional atom probe data. The balance of each analysis is nickel and the data are in atomic percent

Phase	Heat treatment	Cr	Fe	Nb	Mo	Ti	Al	Co
γ	A + 2012 h at 873 K	27.0	26.2	0.58	2.26	0.19	0.22	0.25
	AC + 2012 h at 873 K	23.8	25.6	0.52	2.54	0.13	0.19	0.38
Primary γ''	AC + 500 h at 873 K	2.00	1.43	16.0	2.38	5.36	0.31	0.39
γ'	A + 2012 h at 873 K	0.33	1.56	8.75	0.31	5.85	10.6	0.21
	AC + 2012 h at 873 K	0.59	1.57	8.21	1.22	3.85	9.28	0.30
γ''	A + 2012 h at 873 K	1.75	1.29	16.6	1.56	3.75	0.43	0.17
	AC + 2012 h at 873 K	1.98	0.81	20.6	2.37	3.68	0.40	0.20

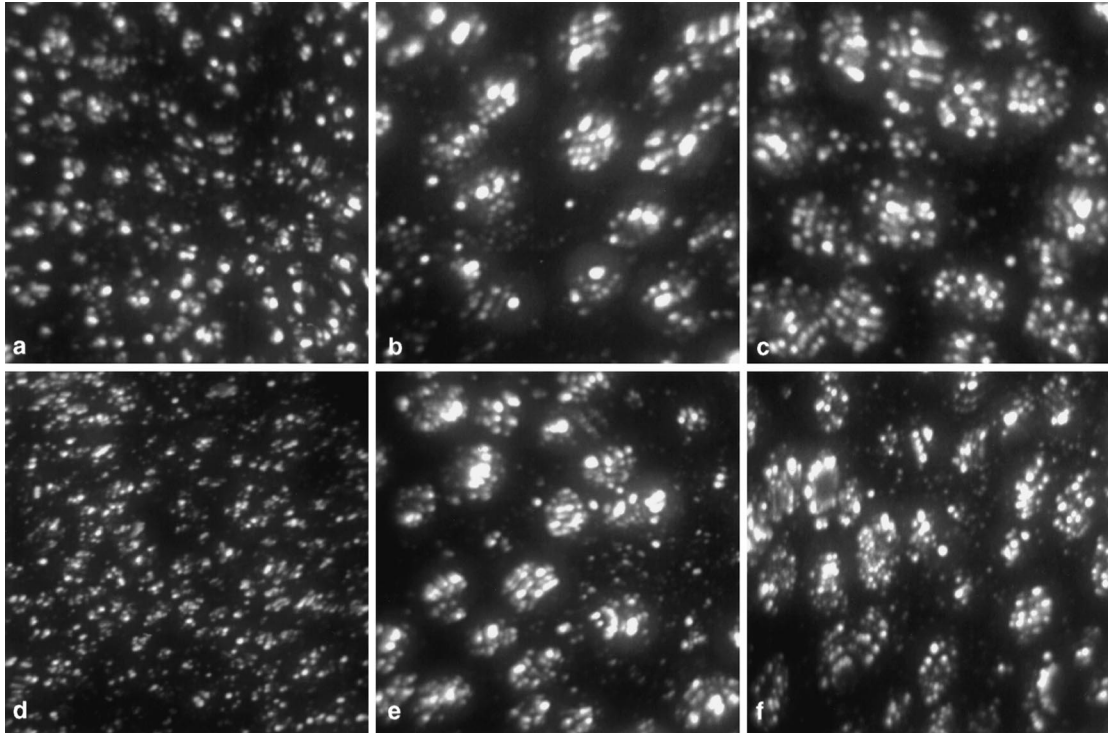


Fig. 8. A series of field ion micrographs showing the evolution of the secondary precipitates during isothermal annealing of alloy 718 at 600°C (873 K). (a) A + 100 h, (b) A + 500 h, (c) A + 2012 h, (d) AC + 100 h, (e) AC + 500 h, and (f) AC + 2012 h.

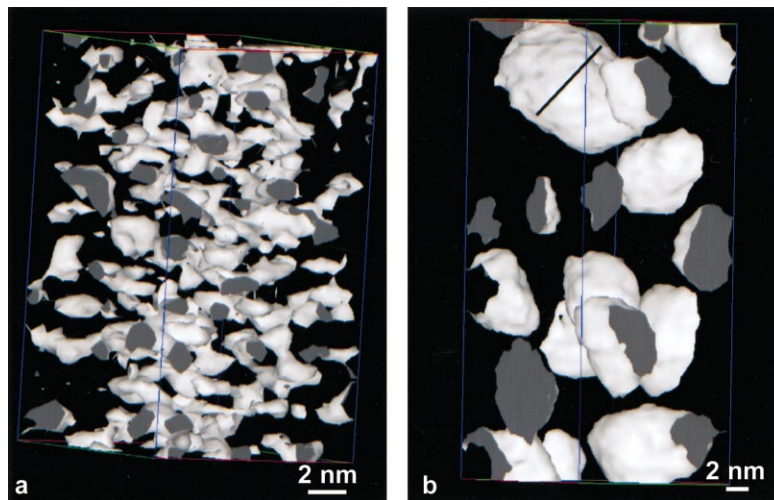


Fig. 9. Isoconcentration surfaces of the secondary precipitates after annealing for (a) 10 and (b) 2012 h at 600°C (873 K).

shown in Fig. 6b. These secondary precipitates are roughly spherical and exhibit similar brightly-imaging contrast to the primary γ'' precipitates in the field ion images.

Some small precipitates were also observed on the surface of the primary precipitates after low temperature annealing at 600°C (873 K), as shown in Fig. 7. The iron plus chromium isoconcentration surface indicates the position of the interface between the primary γ'' precipitate and the γ matrix. The aluminum isoconcentration surface reveals small aluminum-enriched precipitates on this γ'' - γ interface. The morpholo-

gies of these ultrafine precipitates are oblate spheroids that are ~ 4 nm thick by ~ 10 nm diameter. Compositional analysis of these precipitates revealed that aluminum, titanium and niobium partitioned to the precipitate (Ni- 10.6 ± 0.6 at.% Al, $10.5 \pm 0.6\%$ Nb, $6.8 \pm 0.5\%$ Ti, $2.1 \pm 0.3\%$ Fe and $1.6 \pm 0.2\%$ Cr). These precipitates were determined to be the γ' phase from their local compositions.

The alloy was investigated after subsequent isothermal ageing treatments at 600°C (873 K) for times from 10 to 2012 h. A series of field ion micrographs of the secondary

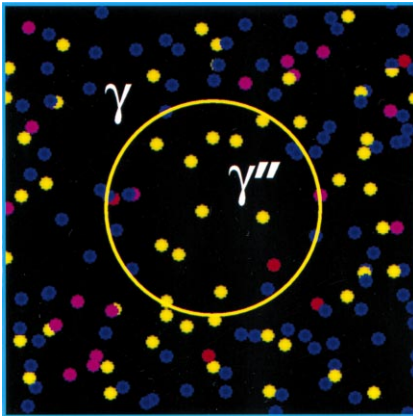


Fig. 10. An atom map of the central portion of a secondary precipitate in alloy 718 isothermally aged for 10 h at 600°C (873 K). The solute distribution indicates that the secondary precipitate (circled) is niobium-enriched indicating that the initial nucleus was the γ'' phase.

precipitates is shown in Fig. 8. The evolution of the secondary precipitates during isothermal annealing at 873 K is shown in the isoconcentration surfaces shown in Fig. 9. After 10 and 2012 h of annealing at 600°C (873 K), the average diameters of the precipitates were determined to be ~ 1.8 and 11 nm, respectively. The coarsening of these secondary precipitates was found to follow a classical t^a power law, where the time exponent a was determined to be 0.34.

An atom map of the central portion of a secondary precipitate in the material isothermally aged for 10 h at 600°C (873 K) is shown in Fig. 10. At the initial stage of precipitation, the solute distribution indicates that the secondary precipitate was niobium-enriched indicating that the initial nucleus was the γ'' phase.

Atom maps of the central regions of two secondary precipitates are shown in Fig. 11.

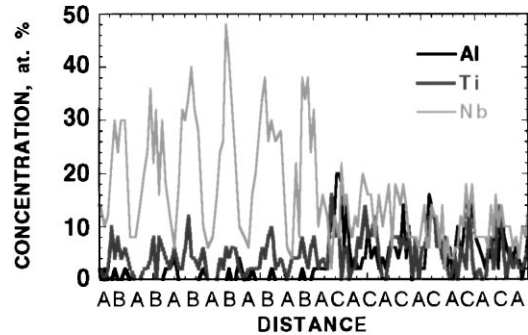


Fig. 12. A composition profile oriented perpendicular to the (001) planes through the central region of a secondary precipitate in alloy 718.

precipitates are shown in Fig. 11. The non-uniform distribution of the niobium, aluminum and titanium atoms indicates that the secondary precipitate consists of two regions of different composition, as shown in Fig. 11a and b. Most of these secondary precipitates exhibited two regions and a small number exhibited three regions. In a few larger precipitates, the aluminum and titanium-enriched region was bounded by two interfaces normal to each other. A composition profile oriented perpendicular to the (001) planes through the central region of a secondary precipitate is shown in Fig. 12 for the material aged for 500 h at 600°C (873 K). The alternating compositions of the (001) layers due to the [AB] DO_{22} - and [AC] $L1_2$ -ordering is clearly evident (where A is a Ni plane, B is a Ni + (Nb,Ti) plane and C is a Ni + (Al,Ti,Nb) plane). The abrupt change in the compositions of the (001) atomic planes (i.e. ABABACACA) indicates that these secondary precipitates are composed of separate γ' and γ'' phase regions. The interface between these regions was determined to be on the $(001)_{\gamma''}/\{001\}_{\gamma'}$ planes. The first mixed C Ni + (Al,Ti,Nb) (001) layer in the γ' after

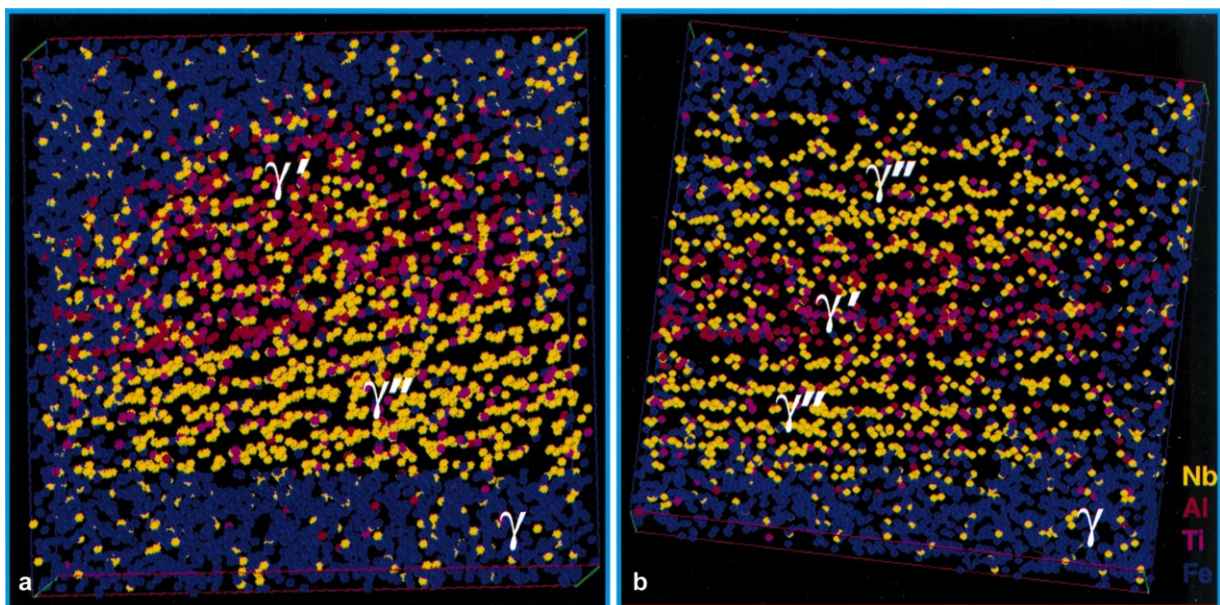


Fig. 11. Atom maps of the central regions of two secondary precipitates in alloy 718.

the DO₂₂-ordered γ'' region was found to be markedly enriched in aluminum. Once established, this dual phase nature persisted for all ageing times examined. No significant discontinuity in the overall envelope of the secondary precipitate was observed at the γ'' - γ' interface as indicated by the isoconcentration surfaces.

The average compositions of these γ'' and γ' phases were determined from selected volume analysis of three-dimensional atom probe data and the results are included in Table 2. The partitioning of the alloying elements among the phases was in good agreement with the thermodynamic predictions.

These atom probe tomography results indicate that the nucleus of the secondary precipitates is the γ'' phase. As the secondary precipitates coarsen, aluminum is rejected from the precipitate and since the solubility of aluminum in the γ matrix is also low, a γ' region is formed on the surface of the secondary precipitate. As ageing proceeds, these two regions grow at the same rate and maintain a smooth envelope to the precipitate.

6. Conclusions

Atom probe tomography has enabled some fine scale details of the microstructures of superalloys to be experimentally determined. Boron, phosphorus and molybdenum enrichments at grain boundaries in a nickel–molybdenum superalloy have been characterized. Fine γ precipitates have been characterized in the central regions of cuboidal γ' precipitates in single crystal PWA 1480. The nature of the secondary precipitates that form in alloy 718 after ageing at 600°C (873 K) has been characterized. Small γ' precipitates were observed on the primary γ'' - γ interface in the material aged at 600° (873 K). The secondary precipitates were found to have regions of γ'' and γ' phases and the interface between these regions was on the $(001)_{\gamma''}/\{001\}_{\gamma'}$ planes.

Acknowledgements

The author would like to thank Drs J.S. Lin and A.D. Cetel of Pratt and Whitney and Drs L.M. Pike and D.L. Klarstrom of Haynes International for providing materials used in this study and Dr I.M. Anderson, S.S. Babu and K.F. Russell for their assistance. Research at the Oak Ridge National Laboratory ShaRE User facility was sponsored by the Division of Materials Sciences and Engineering, US Department of Energy, under contract

DE-AC05-96OR22464 with Lockheed Martin Energy Research Corp.

References

- Babu, S.S., David, S.A., Miller, M.K., 1996a. Microstructural development in PWA-1480 electron beam weld—an atom probe field ion microscopy study. *Appl. Surf. Sci.* 94/95, 280–287.
- Babu, S.S., David, S.A., Vitek, J.M., Miller, M.K., 1996b. Atom probe field ion microscopy investigation of CMSX-4 Ni-base superalloy laser beam welds. *J. de Physique IV, suppl. to J. de Physique III C6*, 253–258.
- Blavette, D., Duval, P., Letellier, L., Guttman, M., 1996a. Atomic-scale APFIM and TEM investigation of grain boundary microchemistry in Astroloy nickel base superalloys. *Acta Mater.* 44, 4995–5005.
- Blavette, D., Letellier, L., Duval, P., Guttman, M., 1996b. Atomic-scale investigation of grain boundary segregation in Astroloy with a three dimensional atom-probe. *Mater. Sci. Forum* 207–209, 79–92.
- Blavette, D., Cadel, E., Deconihout, B., 2000. The role of the atom probe in the study of nickel base superalloys. *Mater. Charact.* 44, 133–157.
- Burke, M.G., Miller, M.K., 1989. APFIM/TEM characterization of precipitation in Alloy 718. *J. de Physique* 50-C8, 395–400.
- Burke, M.G., Miller, M.K., 1991a. Precipitation in alloy 718: a combined AEM and APFIM investigation. In: Loria, E.A. (Ed.), *Proc. Superalloys 718, 625 and Various Derivatives*, June 1991, Pittsburgh, PA. The Minerals, Metals and Materials Society, Warrendale, PA, pp. 337–350.
- Burke, M.G., Miller, M.K., 1991b. Grain boundary intermetallic phases in alloy 718. In: Stocks, G.M., Pope, S.P., Giamei, A.F. (Eds.), *Proc. Alloy Phase Stability and Design*, April 1990, San Francisco, CA, vol. 186. Materials Research Society, Pittsburgh, PA, pp. 215–218.
- Letellier, L., Bostel, A., Blavette, D., 1994a. Direct observation of boron segregation at grain boundaries in Astroloy by 3D atomic tomography. *Scripta Metall. Mater.* 30, 1503–1508.
- Letellier, L., Guttman, M., Blavette, D., 1994b. Atomic scale investigation of grain boundary microchemistry in the nickel based superalloy Astroloy with a 3-dimensional atom probe. *Phil. Mag. Lett.* 70, 189–194.
- Loria, E.A. (Ed.), 1989. *Proc. Superalloy 718*, June 1989, Pittsburgh, PA. The Minerals, Metals and Materials Society, Warrendale, PA.
- Miller, M.K., 1986. Atom Probe Field Ion Microscopy, tutorial presented at the Microbeam Analysis Society, Meeting, Albuquerque, NM.
- Miller, M.K., 1999. Atom probe studies of phase transformations in nickel-based superalloys. In: Koiwa, M., Otsuka, K., Miyazaki, T. (Eds.), *Proc. Int. Conf. Solid–Solid Phase Transformations PTM'99*, Kyoto, Japan, May 1999. The Japan Institute of Metals, Sendai, Japan, pp. 73–76.
- Miller, M.K., 2000. *Atom Probe Tomography: Analysis at the Atomic Level*. Kluwer Academic/Plenum Publishers, New York.
- Miller, M.K., Burke, M.G., 1991. Atom probe analysis of the compositions of γ' and γ'' intermetallic phases in nickel-based superalloy 718. In: Stocks, G.M., Pope, S.P., Giamei, A.F. (Eds.), *Proc. Alloy Phase Stability and Design*, April 1990, vol. 186. Materials Research Society, Pittsburgh, PA, pp. 223–228.
- Miller, M.K., Jayaram, R., Lin, J.S., Cetel, A.D., 1994. APFIM characterization of single-crystal PWA 1480 nickel-base superalloy. *Appl. Surf. Sci.* 76/77, 172–176.
- Miller, M.K., Cerezo, A., Hetherington, M.G., Smith, G.D.W., 1996. *Atom Probe Field Ion Microscopy*. Oxford University Press, Oxford.
- Miller, M.K., Babu, S.S., Burke, M.G., 1999. Intragranular precipitation in alloy 718. *Mater. Sci. Eng. A270*, 14–18.